

Water and Radioactive Tracer Flow in a Heterogeneous Field-Scale System

by Frank M. Dunnivant^{a,b,c}, Meredith E. Newman^{a,b}, Carolyn W. Bishop^a, Dave Burgess^a, John R. Giles^a,
Brian D. Higgs^a, Joel M. Hubbell^a, Erick Neher^a, Greg T. Norrell^a,
M. Cathy Pfeifer^a, Indrek Porro^a, Robert C. Starr^a, and Allan H. Wylie^a

Abstract

A coupled field-scale aquifer pumping and water infiltration test was conducted at the Idaho National Engineering and Environmental Laboratory in order to evaluate subsurface water and contaminant transport processes in a heterogeneous flow system. The test included an aquifer pumping test to determine the storage properties of the aquifer and the state of confinement of the aquifer (~190 m below land surface), and a vadose zone infiltration test to determine vertical moisture and radioactive tracer migration rates. Pump test results indicated that the Snake River Plain Aquifer was locally unconfined with a transmissivity ranging from 5.57×10^5 to 9.29×10^4 m²/day. Moisture monitoring with neutron probes indicated that infiltrating water was initially transported vertically through the upper basalt layer of the vadose zone, primarily through fractures and rubble zones, at an average rate of 5 m/day (based on vertical distance traveled and first arrival of water at the monitoring points). Analysis of breakthrough curves for a conservative tracer allowed estimation of the arrival of the peak concentration and yielded an average velocity of 1 m/day. The migration velocities from the neutron probe and tracer tests are in good agreement given the scale of the test and difference in analysis techniques. None of the data sets showed a correlation between migration velocity (arrival time) and distance from the point source, but they strongly indicate preferential flow through discrete fractures. Upon reaching the first continuous sedimentary interbed layer in the basalt formation, water flow was diverted laterally along the interbed surface where it spread outward in primarily three areas corresponding to topographic lows on the interbed surface, and slowly infiltrated into the interbed. The unpredictable movement of water and tracer through specific fractures underlying the site suggests that a priori prediction of transmissive fractures in this media is not possible. Results do suggest that the continuous sedimentary interbed layers, in general, impede vertical water flow and contaminant migration.

Introduction

A difficult waste management problem facing developed countries today is the safe, long-term disposal and maintenance of nuclear waste. Considerable effort is currently being expended to locate one or more permanent storage facilities within the United States, as well as to understand the transport and fate of radioactive contaminants in existing burial sites. One of the largest subsurface disposal facilities of this type in the United States is located at the Idaho National Engineering and Environmental Laboratory (INEEL) and contains approximately one-third of the U.S. Department of Energy's (DOE) total inventory of plutonium-contaminated waste. Waste at the INEEL resides in the 144,100 m² (88-acre) Subsurface Disposal Area (SDA) within the Radioactive Waste Management Complex (RWMC) and was placed in unlined shallow pits, soil vaults, and trenches in surficial sediments. The waste, disposed during a 32-year period beginning in 1952, contains 31 radioactive contaminants (Arrenholz and Knight 1991; Loehr et al. 1994; EG&G

Idaho Inc. 1994) as well as heavy metals, depleted uranium, asbestos, volatile and nonvolatile organics, and inorganic acids (Loehr et al. 1994). The SDA has been flooded on three separate occasions, in 1962, 1969, and 1982, by local snow melt water during Chinook-type conditions and infiltrating water may have contacted buried waste and promoted subsurface migration. Flood control and diking projects in the 1980s have, thus far, successfully avoided additional large-scale flooding events, although localized flooding may still occur during rapid snow melt and/or intense, short-term precipitation events. Thus, flow responsible for contaminant transport from the RWMC may be described as local intermittently saturated (during periods of high snow melt and flooding events), while the majority of the time the subsurface between land surface and the aquifer (at ~168 m) is unsaturated.

The INEEL burial site is unique in that it is underlain by undulating basaltic lava flows containing interbedded fluvial, lacustrine, and eolian deposits of clay, silt, sand, and gravel. The majority of the upper 168 m, the primary subject of this investigation, is unsaturated. One of the most important questions concerning the transport of radionuclide contaminants at the site is whether sedimentary interbeds in the vadose zone act as hydrologic barriers to water infiltrating to the eastern Snake River Plain Aquifer. The aquifer has been estimated to contain approximately 2.5×10^{11} m³ of recoverable water (Hackett et al. 1986) and thus constitutes a major resource to the state of Idaho. Large-scale field investigations conducted in saturated, fractured media emphasize the complex

^aLockheed Martin Idaho Technologies Co., Idaho National Engineering and Environmental Laboratory, Integrated Earth Sciences, P.O. Box 1625, M.S. 2107, Idaho Falls, ID 83415-2107.

^bCurrent address: Department of Chemistry, Hartwick College, Oneonta, NY 13820.

^cAuthor for correspondence.

Received July 1997, accepted March 1998.

processes involved in the transport of contaminants in fractured media (Neretnieks 1987; Frick et al. 1992). The purpose of the Large-Scale Aquifer Pumping and Infiltration Test (LPIT) was to mimic the intermittent saturated flow events (flooding) potentially responsible for the migration of buried contaminants at the INEEL. The purpose of this article is to summarize and contrast the main elements of the test in one publication and inform the scientific community of the extensive data sets available through the cited Department of Energy publications. These diverse and complementary data sets will be useful to scientists studying flow through similar heterogeneous systems.

The LPIT consisted of several different, but complementary, experiments. Complementary methods were used to reduce data gaps and to provide moisture information in regions between monitoring wells. Results from four of these experiments are summarized in this paper and include: (1) the aquifer pumping test which determined characteristics of the aquifer such as transmissivity, specific yield, and state of confinement, and which also supplied water for the infiltration test; (2) the neutron probe monitoring of primarily vertical water movement in the vadose zone above a sedimentary interbed (located 55 m below land surface and ~113 m above the aquifer); (3) the surface direct-current resistivity monitoring of primarily lateral moisture movement, including spatial location and accumulation of perched water on the 55 m sedimentary interbed; and (4) the water sampling and analyses used to monitor the movement of radioactive tracers through the first 55 m of the vadose zone.

Methodology

General Test Design

Small- or intermediate-scale experiments are of limited value for hydrologic and geologic characterization in a highly heterogeneous environment such as the subsurface beneath the eastern Snake River Plain. In an effort to mimic the physical scale of the subsurface disposal area (144,100 m²) while keeping the experiment to a manageable and economical size, a basin size of 26,300 m² (183 m diameter circular basin containing 32 million liters of water delivered from the test well) was selected. A subsurface monitoring network was set up that contained the basin and the area surrounding the basin, extending down to the 55 m interbed (contained a total monitoring volume of 17,660,000 m³). Diagrams showing the locations of the RWMC, the test well, the infiltration basin (shaded inner circle), monitoring wells in and around the infiltration basin, and the spreading areas for water diverted from the test well are shown in Figure 1. The infiltration basin was located approximately 1400 m south of the RWMC. The circular basin (shaded area in Figure 1) was constructed by removing surface soil that was used to build an earthen berm (1.5 m high) around the area of interest. The floor of the basin was highly uneven. Approximately 80% of the basin floor consisted of a thin layer of soil overlying basalt while the remaining 20% consisted of exposed and elevated basalt. The water depth in the basin ranged from 0.3 to 2 m. The basin was approximately 1.5 km east of the test well, which was both the source of the water to the infiltration basin and the site for the aquifer pumping test (conducted simultaneously with the infiltration test). This distance of separation between the test well and the infiltration basin was based on the estimated region of influence of the test well and was selected to avoid interference between data collection for the aquifer pumping test and water reaching the aquifer

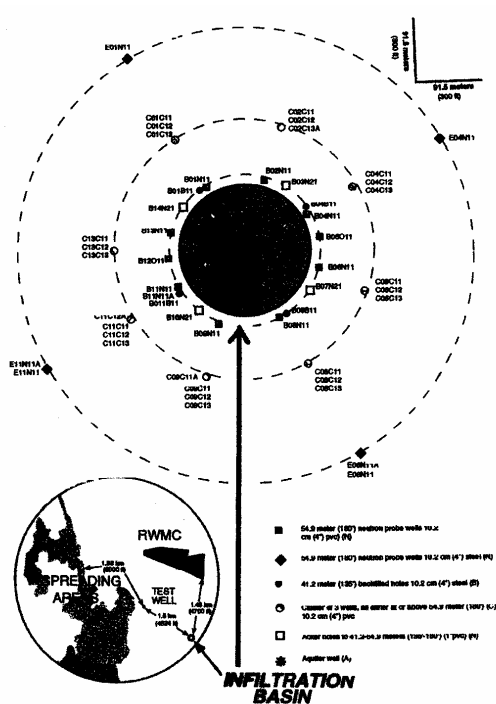


Figure 1. Map showing names and locations of wells, and general layout of the infiltration basin. Inset shows relative location of the RWMC, test well, spreading area for the diverted water, and the infiltration basin (shaded inner circle).

from the infiltration test. Water was pumped from the test well at a rate of approximately 11,000 L/min. Because the infiltration basin could not accept the entire volume of water produced, a diversion pipe was installed to transport excess water to a spreading area approximately 1.8 km west of the test well (Figure 1; the lines and arrows indicate the location of the diversion pipe and the release point of water to the spreading area). The water level in the basin was maintained at a constant "pool-level" (32 million L) except during the addition of tracers to the subsurface. A complete summary of the water management system and water balance during the infiltration test is given in Starr and Rohe (1995).

A total of 70 wells were installed primarily along four axes extending radially from the infiltration basin with a few wells located between these axes (Figure 1). The primary monitoring area of interest was from land surface to the first continuous sedimentary interbed located at a depth of 55 m. Well depths ranged from 15 to 55 m (ground water beneath the basin was at approximately 190 m). Only well A11A31 penetrated the 55-m interbed and terminated in the aquifer at 207 m. Well A11A31 was screened from 165 to 207 m for collection of water samples. Wells in and around the infiltration basin were installed using an air rotary rig with a downhole percussion hammer, and were completed using PVC casing (five wells, for use in the DC resistivity system, were completed with carbon-steel casing). The annular space between the well casing and the borehole was completed using alternating layers of granular bentonite (10 to 20 mesh) and silica sand (6 to 10 mesh).

This type of well completion allowed water to pass freely through fractures or rubble zones, while impeding water movement along the annular space between the well casing and subsurface media in areas dominated by dense basalt. Fractures and dense basalt areas were located by reviewing caliper and video logs of the boreholes. Thus, sand was installed in the annular space when fractures or rubble zones were present, while bentonite was used to seal dense basalt areas between sand completion intervals. Wells were screened only at the bottom, which was usually located at the top of the interbed, to allow collection of water samples. The exact placement of the screen depended upon the presence of fractures, rubble zones, or voids in the area immediately above the interbed. In general, screened intervals ranged from 1 to 3 m immediately above the interbed down to the interbed (refer to Newman [1994] for completion diagrams and the location of all screened intervals). Nested lysimeters, for the collection of water samples, were installed in a similar manner using silica flour and silica sand filling materials immediately adjacent to the lysimeter and sealing between individual lysimeters, and between the lysimeters and land surface, using bentonite (refer to Newman [1994] for completion diagrams and the location of all lysimeters). Five wells and three lysimeter sets inside the basin were evaluated with respect to leakage of water (and ^{75}Se tracer) around the annular bentonite seals over the entire depth of the well. Results from this evaluation are reported in Dunnivant et al. (1997) and show that no leakage occurred; thus, the well installation methods used here appear to be adequate and allow the collection of water from individual fractures. This type of installation also allowed in situ moisture monitoring (with neutron probes) in discrete fractured intervals or rubble zones as well as in dense basalt formations over the entire depth of the wells, and collection of water samples from standing water at the bottom of the well as well as lysimeters located in fracture and rubble zones. Wells were clustered at the intersection of the four axes and four concentric circles moving outward from the basin (shaded area in Figure 1). The first ring of wells (A wells) were located within the basin at approximately 46 m from the basin center. The B, C, and E rings were located at 107, 183, and 320 m, respectively, from the basin center. All of these wells were used in moisture (neutron probe) monitoring and water sampling efforts. Piers were built from the berm out into the basin to provide access to the A-ring wells within the basin.

Water was first pumped into the basin July 25, 1994, at a rate of 11,000 L/min. The basin reached pool level, approximately 31.65×10^6 L (with water depth ranging from 0.3 to 2 m across the uneven surface of the basin), in two days. Tracers (selenium-75, ~ 2.0 Ci total; $t_{1/2} = 119.77$ d, strontium-85, ~ 0.63 Ci total; $t_{1/2} = 64.84$ d, and terbium-160, ~ 3.7 Ci total; $t_{1/2} = 70.3$ d) were added July 31, 1994, as an 11-day finite-pulse input. Background tracer concentrations in the water from the test well were below the detection limit, which would be expected given the short half-lives of the tracers. Tracer addition was accomplished by adding the tracers as a spike to the full basin (approximately 31.65×10^6 L) and mixing the basin using three 7600 Lpm irrigation pumps. During this 11-day period, all water from the test well was diverted to the spreading areas. After the 11-day period, tracer-free water from the test well was again added to the basin and the basin was maintained at pool level through August 30, 1994. This last addition of tracer-free water provided approximately 86×10^6 L of water (or 2.72 times the volume of tracer-containing water) to move the tracers through the subsurface. The net result of this type of tracer addition was a potential broadening of the

breakthrough curves and an increase in observed dispersion coefficients, but this was unavoidable given the scale of the experiment. Laboratory experiments confirmed the conservative (not reactive and adsorbed) nature of selenate for basalt and bentonite systems. Selenium-75 was selected because it should be present as the conservative (not reactive or adsorbed) selenate anion (SeO_4^{-2}) under the conditions of Snake River Plain Aquifer ground water (pH = 8.3, and $E_H = +0.24$ V). Analysis of basin and well water samples did not show a significant change in pH values, and since the water remained oxygenated during the infiltration experiment, ^{75}Se most likely remained present as the selenate anion. Strontium-85 was considered to be present as the free aquated cation and was selected because strontium is a fission product of concern at the RWMC. Terbium-160 was selected as a surrogate for lanthanides that have been disposed at the RWMC, and was expected to be strongly sorbed by INEEL subsurface materials. Laboratory studies indicated strontium had a K_d of 2.0 to 3.0 mL/g and was not expected to be observed at any of the monitoring sites under local equilibrium conditions. However, ^{85}Sr and ^{160}Tb were included to evaluate the presence of preferential flow and nonequilibrium transport in the system.

Aquifer Stress Test

The aquifer stress test was conducted by pumping the test well at an average rate of approximately 11,000 Lpm for 36 days. The test well was drilled to a total depth of 261 m with a cable tool rig and cased to 134 m. The remainder of the well was left as an open borehole with no casing or screen. Two observation wells were installed for this portion of the test; observation well 1 (OW1) was located 33.5 m N30E of the test well, and observation well 2 (OW2) was located 115 m S30E of the test well. The two observation wells were drilled to 304 m and cased to 183 m with a forward rotary drill equipped with a downhole hammer. The remainder of the boreholes were uncased. The water table was located at approximately 190 m below land surface and the presumed base of the aquifer is approximately 427 m below land surface. Drawdown of the aquifer during the pumping test was observed in three wells, OW1, OW2, and well 120 (229 m deep) located 36.6 m west of the test well (refer to the inset in Figure 2). Drawdown was measured in the observation wells using PTX-161D and PXD-260 transducers connected to a HERMIT 1000B and C data logger (In Situ Inc., Laramie, Wyoming). Observed drawdowns were corrected for fluctuations from barometric pressure changes, fluctuations associated with diurnal temperature/barometric pressure changes, and interruptions in pumping due to pump maintenance prior to data analysis. Data from the times when the pump was down for maintenance were deleted; these were short breaks in an otherwise long test.

Neutron Probe Measurements

Water movement and moisture changes in the vadose zone were monitored using 503DR HYDROPROBES (Boart Longyear CPN Co., Martinez, California). Several neutron probes of the same model were used during the test to provide increased coverage of the monitoring wells. Readings from the different probes were correlated to one another using calibration pits with different moisture conditions. This allowed readings made with one probe in a given well to be compared to readings made with other probes in the same well. All measurements during the experiment were made as 16-second counts at 0.30 m increments. All neutron probe wells at the test site were monitored at least once during the month just prior to the experiment to determine background moisture levels.

In most cases, wells were logged several times with several different probes. Sampling frequency of each well varied, and was intensive (approximately every four hours) during the initial portion of the test, but the frequency was reduced (approximately twice a day) as the changes in moisture decreased with time. Measurements made during the test were compared to the appropriate background log measurements to determine if moisture changes were occurring. Raw neutron probe counts were used in the analyses and no attempt was made to calibrate probe counts to water content. At each depth of measurement, a higher number of counts compared to the background level was taken as an increase in moisture. The positive difference between a given reading and the background was considered a real increase in moisture and not just the result of natural variation in readings if the difference continued to increase in subsequent logs. A more detailed description of the neutron probe monitoring can be found in Porro and Bishop (1995).

Direct Current Resistivity

The design for direct current (DC) resistivity monitoring of water infiltration was a bipole-bipole array using a fixed source bipole and a receiver array consisting of 2700 receiver bipoles (Pfeifer and Anderson 1995). The receiver bipole array consisted of a common remote electrode located near the center of the basin and a circular array of 2700 electrodes positioned in the areas between the monitoring wells outside the basin (Figure 1). The potential differences between each of the electrodes outside the basin and the common electrode within the basin were measured resulting in a maximum of 2700 potential difference measurements recorded during each monitoring session.

Water Sampling and Analyses

Water samples were collected on a regular basis from the infiltration basin, monitoring wells, and lysimeters in order to monitor the concentration of tracers in the basin and observe the breakthrough of tracers in the monitoring wells. A detailed account of the sampling methodology is given in Newman (1994) and Newman and Dunnivant (1995) and is only briefly summarized here. Eight locations within the infiltration basin were sampled using plastic containers. Well samples were collected using bottom-loading polyethylene bailers. Lysimeters were sampled by applying a vacuum of 65 to 70 kPa and allowing the lysimeter to collect water for 24 hours or until the tension in the lysimeter was approximately 35 kPa. The lysimeters were pressurized with bottled nitrogen or helium to evacuate the sample to land surface. Samples were analyzed on site in a mobile laboratory. Sample analyses included pH, specific conductivity, and radioactive tracers (^{75}Se , ^{85}Sr , and ^{160}Tb). Gamma spectroscopy for ^{75}Se , ^{85}Sr , and ^{160}Tb was performed using a high purity germanium system. Energy-line, full-width, half-maximum calibrations and background verifications were run each day prior to sample analysis. Specific conductivity and pH were analyzed using standard meters, cells, and electrodes. Instruments were calibrated once every two hours or prior to use.

Results and Discussion

Aquifer Stress Test

The aquifer pumping test was conducted to determine transmissivity, specific yield, and the state of confinement of the aquifer, as well as to supply water for the infiltration test. First, we will discuss the barometric "efficiency" of the well, which relates to the effectiveness of the pressure transmittal and is dependent upon

the rigidity of the geologic media and the overall permeability of the rock. Typically the potentiometric surface of a confined aquifer is not affected directly by barometric pressure changes, so barometric pressure changes have a direct, measurable impact only on water levels in wells. However, the potentiometric surface of an unconfined aquifer is usually in direct contact with the atmosphere; hence, barometric pressure changes have a negligible impact on water levels in wells. Prior to the LPIT the barometric efficiency for well 120 in the Snake River Plain Aquifer was found to be approximately 90% for short-term fluctuations and 60% for long-term fluctuations, suggesting that the aquifer is confined (Wylie et al. 1995). However, data from the large-scale pumping test indicate that the aquifer is unconfined (Figure 2). One possible explanation for this observation is that those geologic units isolating the aquifer from barometric pressure fluctuations are above the potentiometric surface of the aquifer and do not act as aquitards. Our conceptual model is that aquifer permeability is largely controlled by the distribution of basalt flow contacts with some additional permeability contributed by fractures, vesicles, and intergranular pore spaces (Mundorff et al. 1964). Individual basalt flows within the Snake River Plain Aquifer consist of four elements: an upper vesicular element, a central nonvesicular element, a bottom vesicular element, and a substratum. The observed median thicknesses of the three upper elements are 1.8, 2.3, and 0.46 m, respectively (Knutson et al. 1989). On the scale of the aquifer test (hundreds of meters), dense basalt flow interiors act as "grains" while the "intergranular porosity" is reflected in the interflow zones between the dense interior (Whitehead 1992). These "grains" are formed as basalt flow sequences are deposited in an overlapping and coalescing manner, where younger flows build on the complex undulating topography of previous flows. Flow through the aquifer follows a tortuous path, around, through, and between these large particles in the general direction of the regional hydraulic gradient. If a well is open below the water table, or if the potentiometric surface is within a section of dense basalt, and the potentiometric surface is insulated

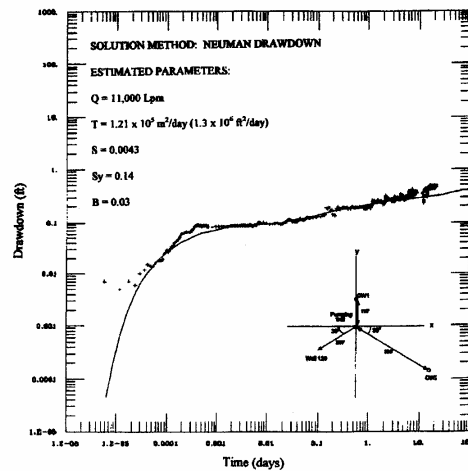


Figure 2. Neuman analysis of time-drawdown plot of well 120 data. The solid line represents the fitted curve. T = transmissivity, S_y = specific yield, S = storativity, and Q = pumping rate.

O
W
O
r
O
r
W
r
O
r
A
fro
res
ing
su
ch:
inc
pu
Ne
do
rec
fr
10
10
pr
th
ple
po
is
pe
in
At
ity
wi
th
an
cal
lyt
Ne
an
pr
re:
sa
ba
lit
oc

Observation Well	Transmissivity (m ² /day)	Storage	Kh/Kv Ratio	Analytical Method
OW1 upper r = 33.5 m	1.39 × 10 ⁵	1.3 × 10 ⁻¹	1 × 10 ²	Neuman drawdown Theis recovery
	5.48 × 10 ⁵	5.3 × 10 ⁻²		
OW1 lower r = 33.5 m	5.11 × 10 ⁵	1.8 × 10 ⁻¹		Neuman drawdown Theis recovery
	3.25 × 10 ⁵	2.3 × 10 ⁻²		
Well 120 r = 60.96 m	1.21 × 10 ⁵	1.4 × 10 ⁻¹	6 × 10 ¹	Neuman drawdown Theis recovery
	1.11 × 10 ⁵	5.0 × 10 ⁻²		
OW2 upper r = 115.2 m	1.39 × 10 ⁵	1.4 × 10 ⁻¹	3 × 10 ¹	Neuman drawdown Theis recovery
	7.25 × 10 ⁵	4.2 × 10 ⁻²		
All wells	1.30 × 10 ⁵	9.0 × 10 ⁻²		Distance drawdown

from barometric pressure changes, a barometric pressure change will result in a pressure difference between the well and aquifer, causing the water in the well to either rise or fall in response to the pressure difference.

The water level change is inverse to the barometric pressure change; if barometric pressure decreases, the water level will increase. Analytical results (Newman and Theis methods) for the pump test data presented in Figure 2 are summarized in Table 1. The Newman method was used to obtain estimates from the drawdown portion of the curve and the Theis method was used for the recovery portion of the curve. Estimates of transmissivity vary from 9.29×10^4 m²/d to 5.57×10^5 m²/d (1×10^6 ft²/d to 6×10^6 ft²/d) and the storage coefficient varies from 1×10^{-1} to 2×10^{-2} . The observed drawdown in the test well was 2.90 m, while the predicted drawdown using calculated aquifer coefficients from this test is 0.17 m. The well efficiency is 6%, yet the test well is completed as an open hole. An open hole is the most efficient well design possible. Perhaps the well efficiency is low because permeability is not evenly distributed throughout the length of the well. Aquifer permeability may be isolated in the basalt flow contacts, resulting in converging and turbulent flow within and adjacent to the well. Attempts to match the data with the Moech (1984) double porosity model yielded higher permeabilities within the matrix blocks than within the fractures. Perhaps the data are adequately described by the Neuman model because the matrix material is sufficiently low and the interflow zones are distributed evenly enough that fluid flow can be approximated with an equivalent porous granular media analytical model.

Neutron Probe Moisture Monitoring

Water movement in the fractured basalt vadose zone beneath and adjacent to the infiltration basin was monitored using neutron probes during the LPIT. Wetting fronts and wetted zones were readily distinguished using these probes. Moisture changes in the sand and bentonite used to fill the annular space between casing and basalt in the monitoring wells could also be detected during equilibration with antecedent vadose zone moisture. These changes occurred during the first few months after well completion and prior

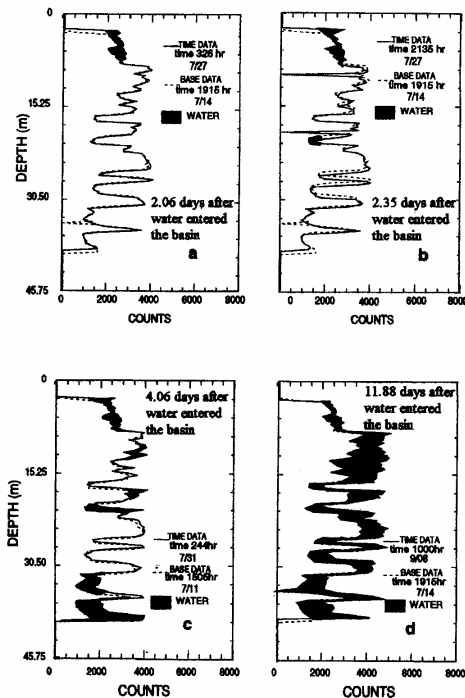


Figure 3. CPN (moisture monitoring) results from well A11C12 (inside the infiltration basin) illustrating the wetting progression from (a) 2.06 days after the addition of water to (b) 2.35 days after the addition of water to (c) 4.06 days after the addition of water to (d) 11.88 days after the addition of water to the basin. The dashed line in each plot represents the background neutron log while the solid line represents data collected on the specified day. Deviations between the two data sets are indicated by shaded areas.

to the LPIT so equilibrium was reached before infiltration was initiated. These observations indicate that vadose zone wells constructed in this manner and used in this type of subsurface environment should be installed and allowed to equilibrate sufficiently before they are used for moisture measurements.

In general terms, vertical water flow in the vadose zone during the infiltration test was confined within a cylinder directly beneath the infiltration basin. The rate of the wetting front advance averaged about 5.0 m/day ($n = 38$, ranging from 1.4 to 17.7 m/day, $s.d. = 2.90$). Although vertical water movement appeared to occur within a cylinder defined by the basin, wetting did not progress as a front uniformly distributed across this area. This is shown in neutron logs given in Figure 3. Figure 3 illustrates the general pattern of wetting observed in the infiltration basin monitoring wells. The shaded areas indicate where moisture levels have increased above background levels due to infiltration from the basin. Initial wetting was observed immediately underneath the infiltration basin to a depth of about 9 m (Figure 3a). Subsequently, a wetted zone appeared at the 19.8 to 21.4 m depths, while measurements between the 9 to 19.8 m depths remained unchanged from background levels (Figure 3b). Clearly, the water must have moved through preferential pathways to

reach the 19.8 to 21.4 m depths without wetting the zone from 9 to 19.8 m; it did not migrate downward uniformly through the geologic material surrounding the well. Figure 3c shows that water reached the 30.0 to 39.7 m depths while bypassing the 25.9 to 32.0 m depths, further illustrating preferential flow. A new wetted zone also appeared around the 12 m depth. Figures 3a to 3c illustrate water moving through the faster flowpaths. Figure 3d shows that 11 days after pumping entered the basin, wetting was evident throughout the entire length of the monitoring well. Water has obviously made its way more slowly through other pathways to wet those zones that were bypassed previously. While there was evidence of preferential and lateral flow within the cylinder beneath the basin, lateral flow did not extend to the B-ring wells just outside the basin, except in the region immediately above the 55 m sedimentary interbed. Moisture level changes were not observed at depths between land surface and the sedimentary interbed in any of the B-, C-, and E-ring wells, except in the media immediately above the interbed where water flowed along topographical lows.

Water movement through a few preferred pathways is suggested by the wetted porosity (0.02%). The wetted porosity was calculated by dividing the average infiltration rate (approximately 11 cm/day) by the wetting front travel rate (approximately 5 m/day). This compares to an average effective porosity of 0.23, which was averaged from 71, 5.6 cm long vesicular basalt cores taken from this area (Bishop 1991). This value was determined for a vesicular matrix without obvious fractures, and the presence of fractures and rubble zones in the field test should cause the porosity to increase. Thus, less than 10% of the total porosity actually conducted water. Bishop (1991) also found an average saturated hydraulic conductivity of 1.6×10^{-8} m/s for a 50 cm \times 20 cm \times 20 cm block of unfractured vesicular basalt. The much faster advance of the wetting front in the large-scale field test indicates that the basalt matrix played a minimal role in conveying water through the vadose zone and that fractures and rubble zones constituted the primary pathways.

Direct Current Resistivity

DC resistivity arrays are commonly used to map changes in the electrical properties of the subsurface due either to geological spatial changes or to changes in physical properties over time. The electrical properties measured are related to the moisture content of the medium so that changes in the DC resistivity measured over time can be used to monitor wetting or drying fronts (Pfeifer 1987; Ash and Morrison 1989; Truskowski 1994). Using this concept, a DC resistivity array was used to monitor the lateral movement of water outward from the infiltration basin. The array was designed to augment well data and to provide real-time coverage of the areas between the sampling wells. The areal extents needed to be covered in real time were large, and to expedite this process, only real-time lateral migration information could be obtained using the DC resistivity array configuration. However, well data were used to determine the depth of the lateral migration of water.

Real-time interpretation of the data was performed in the field and consisted of comparing the data collected during the test with background data collected prior to filling the basin with water. Interpretation consisted of two steps. The first step was to detect anomalous regions in the subsurface geology and the second step was to monitor changes in the potential electric field that could be related to the lateral spreading of water from the basin. First, a map of anomalous areas was generated using the data from each of the electrodes. The geology of the area was modeled using a layered

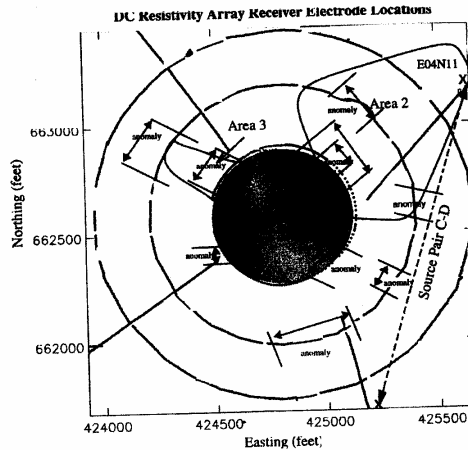


Figure 4. Map of anomalies detected by DC resistivity array superimposed on receiver array positions. Areas 1, 2, and 3 are areas corresponding to changes in the potential field due to lateral water migration. Note that the orientation of this figure is identical to Figure 1.

earth model; anomalous areas are those regions where the data diverged from the layered earth model indicating the presence of three-dimensional geologic structures such as rubble zones, depressions in the top of the interbed, and similar structures. Figure 4 is an areal summation of the geologic anomalies superimposed on the receiver array positions. The anomalous areas were postulated to be areas where lateral movement of water would occur. After mapping the geologically anomalous areas, the array was monitored over the course of the test to detect the lateral movement of water. As expected, the ring of electrodes directly adjacent to the infiltration basin showed the first changes in the anomalous areas. One anomalous area adjacent to the northeastern edge of the basin berm and well B04N11 (designated Area 1 on Figure 4) showed a marked decrease in the potential electric field over time after the addition of water to the basin and prior to the arrival of water in well B04N11. This area was interpreted to be an area of lateral movement of water and the interpretation was confirmed by recovery of water from well B04N11. Monitoring the array farther from the basin showed two areas where changes in the potential were measured. Area 2 (Figure 4) on the northeastern side of the basin coincides with a geologic anomaly and several wells from which water was recovered and was interpreted as a broad area of lateral water movement along the top of the interbed. The second area (Area 3 on Figure 4) is located on the western side of the basin near well B01N11 and is interpreted as a narrower zone of lateral water migration along the top of the interbed. Confirmation of perched water by water sampling could not be made in this area because wells could not be completed to the top of the interbed due to the presence of a large, subsurface rubble zone. Well B01N11 was the only well on the western side of the basin where water was recovered; however, the array data shows the migration of water in this area. In summary, water appeared to move laterally across the interbed surface and outward from the basin primarily in three areas coinciding with areas of geologic anomalies.

Wa
san
We
tion
ten
loc
nat
ly
str
det
mc
of
La
fo
an
as
lir

Al
lal
be
br
pe
—

Water Sampling and Analyses

Each of the monitoring wells and lysimeters was frequently sampled in an effort to collect infiltrating water containing tracers. Wells were sampled at least once every 12 hours after the first detection of water. Lysimeters were sampled every 24 hours or when the tension fell below 35kPa. Of the 101 possible water sampling locations, water was recovered from only 30 and ⁷⁵Se-labeled selenate was detected in 26 of these 30. Nineteen of the 26 wells and lysimeters found to contain tracer produced sufficient data to construct breakthrough curves (BTCs). Neither ⁸⁵Sr nor ¹⁶⁰Tb were detected in any well or lysimeter water sample. However, in situ monitoring with a downhole HPGe detector suggested the presence of ⁸⁵Sr in a few selected zones (Dunnivant et al. 1994, 1997). Lack of detection of ⁸⁵Sr and ¹⁶⁰Tb in water samples indicated that, for most sampling locations, sufficient contact between the tracers and subsurface materials occurred to retard their transport. However, as previously mentioned, preferential flow may have occurred at a limited number of locations.

Representative BTCs from B-ring wells are shown in Figure 5. Although the BTCs obtained were all for the same tracer (⁷⁵Se labeled selenate), the shapes of the BTCs varied significantly between different wells and lysimeters. This dissimilarity between breakthrough curve shapes indicated that a variety of different flowpaths ranging from individual fractures to interconnecting flowpaths

were present beneath the basin. Figures 5a and 5b show the more classical shaped BTCs represented by the Gaussian or bell shape. Figures 5c and 5d show two BTCs (or one bimodal curve) at one location and can be explained by the presence of two separate flow channels between the basin and monitoring point. It is interesting to note the difference in shapes for each of the bimodal BTCs, specifically the width, which is related to dispersion. Specific conductivities of the sampled water are also shown in Figure 5 and confirm the different source (with respect to flowpath) of each water.

A common feature of the BTCs was tailing during the washout phase of the test. Tailing could have been caused by (1) transport in multiple fractures or rubble zones, (2) matrix diffusion, or diffusion from dead-end pores, (3) wall effects in fractures or rubble zones, (4) channeling, (5) mixing in the wells or lysimeters, and (6) the type of tracer input pulse used. Although mixing in the wells and lysimeters was possible, it is doubtful that it was the primary cause of the observed tailing because the degree of tailing varied considerably from well to well and from lysimeter to lysimeter with no apparent relationship between depth of standing water in the wells and degree of tailing observed. It is not possible from the current data set to isolate with certainty which of the first six possible causes was primarily responsible for the observed tailing. It is possible that the observed tailing resulted from a combination of all of these causes.

Several aspects of the data collected confirm the highly complex nature of the system under study. For example, tracer-free water was added to the infiltration basin for six days prior to the addition of tracers; however, the first water observed in several wells contained tracer (Figure 5e and f). Also, tracer-free water was observed in several lysimeters throughout the course of the test. Intervals containing insufficient water for the collection of samples were observed between water bearing zones. In addition, little correlation was observed between distance from the tracer source and tracer arrival time. Arrival times observed for B-ring wells, which were all the same distance from the tracer source, varied from 14.5 to 36.4 days. Results from nested lysimeters showed early arrival of ⁷⁵Se-labeled selenate at a given location while shallower and deeper lysimeters in the same installation showed significantly later arrival times.

One explanation for the diversity of BTCs and the lack of selenate at some monitoring points is the presence of dead-end fractures and fractures or dense basalt zones not directly or continuously connected to the flow of water. It is possible that some dead-end fractures intercepting the sampling points filled with tracer-free water early in the test, causing subsequent water flow at the origin of the flowpath to be diverted to an adjacent fracture or flowpath. The concomitant arrival of water and selenate at a monitoring point may be due to this diversion of water from these "filled" dead-end flowpaths or short circuiting in the system. These proposed flowpaths are illustrated in Figure 6.

Ten ⁷⁵Se breakthrough curves were analyzed using a modification of the one-dimensional advective-dispersive transport model (CXTFIT) of Parker and van Genuchten (1984). The nonreactive, one-dimensional model was selected since the flow regime between land surface and the 55 m interbed is best represented by channel flow through fractures and rubble zones. Basically, this program fits the one-dimensional model to the data set and estimates the most probable water velocity and dispersion coefficient. Results from this modeling effort are summarized in Table 2, while a detailed summary of this approach may be found in Dunnivant and Newman

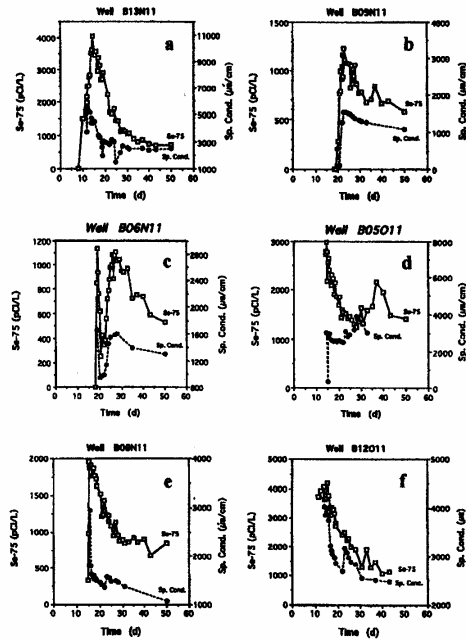


Figure 5. Examples of BTCs for Se-75 labeled selenate and electric conductivity measurements from B-ring wells. Note that time zero in these plots corresponds to the date of tracer addition (July 31, 1994) and not to initial water input to the basin. Figures a and b represent symmetrical or nearly symmetrical BTCs for ⁷⁵Se. Figures c and d represent bimodal BTCs for ⁷⁵Se. Figures e and f represent "unexpected" BTCs for ⁷⁵Se where the first water arriving at the monitoring site contained the highest concentration of ⁷⁵Se.

Location	Vertical Distance (m) from Land Surface	V (m/d) (Estimates from CXTFIT)	Dispersion (m ² /d) Coefficient (Estimates from CXTFIT)	r ² (Regression Coefficient)	Calculated Dispersivity (m) (Dispersion Coefficient Times Velocity)
Lysimeters			0.079	0.8317	0.18
A01B11	6.38	0.45	0.55	0.9067	0.69
A08B11	7.60	0.80	0.68	0.9287	1.19
A08B11	11.55	0.57	1.01	0.9432	1.43
A11B11	14.63	0.71	3.52	0.9018	3.92
A11B11	21.34	0.90	4.15	0.9219	1.58
A11B11	31.62	2.63			
Average		1.01			
Wells			209.0	0.8850	45.80
B04N11	68.67	4.56	0.75	0.8862	0.10
B06N11	68.67	7.52	11.1	0.7064	4.48
B06N11	68.67	2.48	79.1	0.8491	14.40
B13N11	68.67	5.51			
Average		5.02			

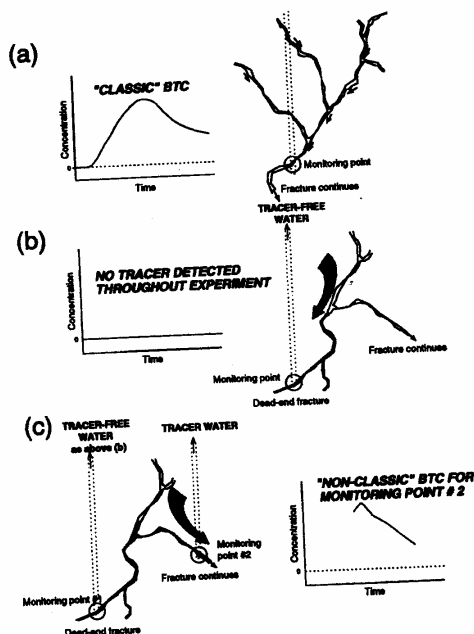


Figure 6. Conceptualization of the subsurface fractures and water flow beneath the basin.

(1996). The model estimated that dispersion coefficients for the fractured basalt regions above the interbed range from 0.079 to 4.15 m²/d (mean = 1.66 m²/d, s.d. = 1.72, n = 6), which correspond to longitudinal dispersivity values ranging from 0.176 to 3.92 m (mean = 1.5 m, s.d. = 1.29, n = 6). Water migration velocity (V in Table 2) estimates range from 0.45 to 2.63 m/d (mean = 1.01 m/d, s.d. = 0.81, n = 6). These predicted water velocities are in reasonable agreement

with the rate of wetting front advance estimated from neutron probe measurements, especially considering that the velocity estimated from neutron probe measurements is for initial wetting while water samples could not be collected until near saturation conditions were reached, and therefore provide estimates of saturated interstitial velocity.

Results for water flow along the interbed are more difficult to interpret since water first flows through one or more fractured basalt regimes, and upon reaching the interbed flows along topographical lows. Under these conditions, the system is no longer one-dimensional and the flowpath length is the sum of the vertical and horizontal distance from the basin floor to the monitoring point. Water velocities to the B-ring wells range from 2.48 to 7.52 m/d (mean = 5.02 m/d, s.d. = 2.09, n = 4). Dispersion coefficients range from 0.75 to 209 m²/d (mean = 27.7 m²/d, s.d. = 35.12, n = 4) and correspond to dispersivity values ranging from 0.10 to 45.8 m (mean = 16.2 m, s.d. = 20.6, n = 4).

Conclusions

The large-scale aquifer pumping and infiltration test provides the INEEL with a valuable data set for evaluating fate and transport of buried wastes at the RWMC, and also provides a unique data set for researchers interested in migration of water through intermittently saturated heterogeneous systems. Data from the pumping test indicate that the Snake River Plain Aquifer is highly transmissive (1.2×10^5 m²/d), although water primarily flows from a few highly productive fractures, and is locally unconfined. Data from moisture and tracer monitoring in the vadose zone are summarized in the conceptualization shown in Figure 7. Water appeared to migrate downward through isolated fractures within a cylinder defined by the infiltration basin and did not spread horizontally outside the basin until reaching the 55 m interbed. The average rate of vertical water transport to the 55 m interbed was 5.0 m/day based on neutron probe results and was 1.0 m/day based on analysis of ⁷⁵Se BTCs. The difference in these two values is probably due to the use of the first arrival of water in the neutron probe technique, while the ⁷⁵Se-based technique used the mid-point of the BTC to estimate water velocity. These BTCs indicate that a variety of subsurface flowpaths exist, ranging from individual fractures to a complex series of intercon-

54.9 m

Figur

necte
lysin

inter
by I
wat
prin
with
wel
mig
intr
has

pre
dis
M
tic
of
if

A

o
c
c
I
c

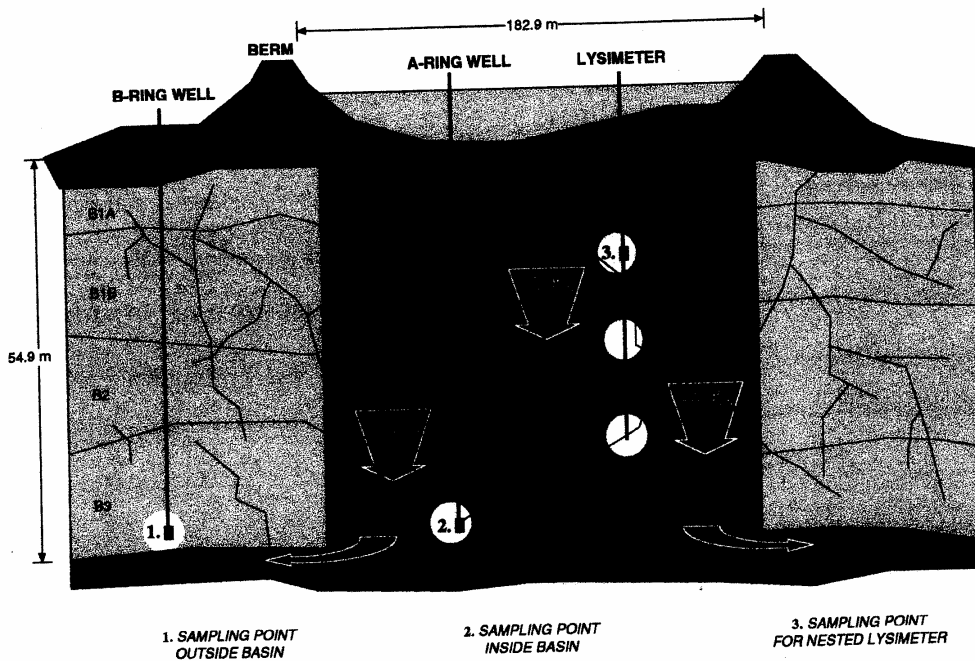


Figure 7. Conceptualization of the overall water flow beneath the basin. B1A, B1B, B2, and B3 represent individual basalt flow units.

nected flowpaths. Not all fractures intercepting monitoring wells or lysimeters produced water or tracer.

As the infiltration test progressed, water reached the 55 m interbed and formed a perched water body that was characterized by DC resistivity measurements and confirmed by recovery of water from monitoring wells. Water moved outward from the basin primarily in three areas coinciding with geological anomalies and with topographic lows on the interbed surface as determined from well logs. In addition, the 55 m interbed appears to impede the migration of water (and tracers). The presence of two similar interbeds below the RWMC suggests that buried waste in the SDA has probably not migrated to the aquifer.

Additional efforts, using an inverse modeling approach, to predict the spatial movement of moisture and estimate the range of dispersivity coefficients in these fractures are summarized in Magnuson (1995) and will be the subject of a subsequent publication. One clear result from this investigation is that a priori prediction of discrete water movement and tracer concentrations is difficult, if not impossible, in the fractured system underlying the INEEL.

Acknowledgments

A test of this magnitude required the efforts of a large number of people. We would like to acknowledge the U.S. DOE-ID, especially Patti Kroupa; program management by Kirk Dooley and Gary Mecham; water sampling by Steve Ugaki, Scott Barrie, and Hollie Gilbert; day-to-day oversight in the field by Pat Boyd, Joe Cook, and Tom Wood; DC resistivity assistance by Denise Psesser

and Andy Anderson; numerous tasks performed by 30 dedicated summer students; and Jackie Brower for drafting of figures. This work was supported by the U. S. Department of Energy, Assistant Secretary for Environmental Management, under DOE Idaho Operations Office Contract DE-AC07-94ID13223.

References

- Arrenholz, D.A., and J.L. Knight. 1991. A brief analysis and description of transuranic wastes in the subsurface disposal area of the radioactive waste management complex at the INEEL. Report no. EGG-WTD-9438. Idaho Falls, Idaho: U.S. Department of Energy, Idaho Operations Office.
- Ash, T., and H.F. Morrison. 1989. Mapping and monitoring electrical resistivity with surface and subsurface electrode arrays. *Geophysics* 54, 235-244.
- Bishop, C.W., 1991. Hydraulic properties of vesicular basalt. M.S. thesis, Dept. of Hydrology and Water Resources, University of Arizona, Tucson, Arizona.
- Dunnivant, F.M., and M.E. Newman. 1996. Migration of radionuclide tracers through fractured media: Preliminary modeling results of breakthrough curves obtained during the large-scale aquifer pumping and infiltration tests. Engineering Design File ER-WAG7-84, INEEL Report no. INEEL-96/0288. Idaho Falls, Idaho: Idaho National Engineering Laboratory.
- Dunnivant, F.M., I. Porro, C.W. Bishop, J. Hubbell, J.R. Giles, and M.E. Newman. 1997. Verifying the integrity of annular and back-filling seals for monitoring wells. *Ground Water* 35, no. 1: 140-148.
- Dunnivant, F.M., G.D. Mecham, and J. Giles. 1994. Results from the large scale aquifer pumping and infiltration test: Down-hole gamma spectroscopy monitoring. Engineering Design File ER-WAG7-54, Report no. INEEL-94/064. Idaho Falls, Idaho: Idaho National Engineering Laboratory.

- EG&G Idaho Inc. 1994. A comprehensive inventory of radiological and nonradiological contaminants in waste buried in the subsurface disposal area of the INEEL RWMC during the years 1952-1983. Report no. EGG-WM-10903. Idaho Falls, Idaho: U.S. Department of Energy, Idaho Operations Office.
- Frick, U., W.R. Alexander, B. Baeyens, P. Bossart, M.H. Bradbury, C. Buhler, J. Eikenberg, T. Fierz, W. Heer, E. Hoehn, I.H. McKinley, and P.A. Smith. 1992. Grimsel test site, the radionuclide migration experiment—Overview of investigations 1985-1990. Paul Scherrer Institute, Wurenlinger and Villigen, CH-5232 Switzerland Villigen PSI, PSI-Report no. 120.
- Hackett, B., J. Pelton, and C. Brockway. 1986. Geohydrologic study of the Eastern Snake River Plain and the Idaho National Laboratory. Idaho Falls, Idaho: US-DOE, Idaho Operations Office.
- Loehr, C.A., B.H. Becker, D.E. Burns, R.M. Huntly, S.M. Rood, P. Sinton, and T.H. Smith. 1994. Preliminary scoping risk assessment for waste pits, trenches, and soil vaults at the subsurface disposal area, INEEL. Report no. EGG-WM-11181. Idaho Falls, Idaho: U.S. Department of Energy, Idaho Operations Office.
- Knutson, C.F., K.A. McCormick, R.P. Smith, W.R. Hackett, J.P. O'Brien, and J.C. Crocker. 1989. RWMC vadose zone basalt characterization. EGG-WM-8949. Idaho Falls, Idaho: Idaho National Engineering & Environmental Lab.
- Magnuson, S.M. 1995. Inverse modeling for field-scale hydrologic and transport parameters of fractured basalt. Report no. INEEL-95/0637. Idaho Falls, Idaho: U.S. Department of Energy, Idaho Operations Office.
- Moench, A.F. 1984. Double-porosity model for a fissured groundwater reservoir with fracture skin. *Water Resources Research* 20, no. 7: 831-846.
- Mundorff, M.J., E.G. Crosthwaite, and C. Kilburn. 1964. Groundwater for irrigation in the Snake River Basin in Idaho. Water Supply Paper 1654, 224. Reston, Virginia: U.S. Geological Survey.
- Neretnieks, I. 1987. Channeling effects in flow and transport in fractured rocks—Some recent observations and models. In *Proceedings of GEOVAL-87 International Symposium*. Stockholm: Swed. Nucl. Inst.
- Newman, M.E. 1994. Integrated large-scale aquifer pumping and infiltration tests—Water sampling and analysis test plan. Report no. EFF-ER-11367. Idaho Falls, Idaho: U.S. Department of Energy, Idaho Operations Office.
- Newman, M.E., and F.M. Dunnivant. 1995. Results from the large-scale aquifer pumping and infiltration test: Transport of tracers through fractured media. Report no. INEL-95/146. Idaho Falls, Idaho: Idaho National Engineering Laboratory.
- Parker, J.C., and M. Th. van Genuchten. 1984. Determining transport parameters from laboratory and field tracer experiments. Agricultural Experiment Station, Bull-Agric. Exp. Stat. No. 84-3, 1-97. Blacksburg, Virginia: Virginia Polytechnic Institute and State University.
- Pfeifer, M.C. 1987. Multi-component underground DC resistivity study at the Waste Isolation Pilot Plant. M.S. thesis T3372, Dept. of Geophysics, Colorado School of Mines, Golden, Colorado.
- Pfeifer, M.C., and H.T. Anderson. 1995. Electrical resistivity monitoring during the aquifer pumping and infiltration test. Report no. INEEL-95/010. Idaho Falls, Idaho: Idaho National Engineering Laboratory.
- Porro, I., and C.W. Bishop. 1995. Large-scale infiltration test CPN data analysis. Report no. INEEL-95/040. Idaho Falls, Idaho: National Engineering Laboratory.
- Starr, R.C., and M.J. Rohe. 1995. Large-scale aquifer stress test and infiltration test: Water management system operation and results. Report no. INEEL-95/059. Idaho Falls, Idaho: Idaho National Engineering Laboratory.
- Truskowski, M.G. 1994. Detecting material property changes and fluid flow using a stationary DC resistivity grid. M.S. thesis T4490, Dept. of Geophysics, Colorado School of Mines, Golden, Colorado.
- Whitehead, R.L. 1992. Geohydrologic framework of the Snake River Plain regional aquifer system, Idaho and Eastern Oregon. U.S. Geological Survey Professional Paper 1408-B.
- Wylie, A.H., J.M. McCarthy, E. Neher, and B.D. Higgs. 1995. Large-scale aquifer pumping test results. Report no. INEEL-95/012. Idaho Falls, Idaho: Idaho National Engineering Laboratory.

T

Abstr
TI
for con
tance (c
lytical
cumul
type c
opment
the dir
are th
through
inwar

Intro
In
neousl
sion. A
nated,
and tr
advect
could l
insigni
simult
the mc
siderat
optimi
there i
persio
compu
ual flo
of the
involv
tively
region
approq
zone c

“C
Exton,
bt
08628.
R

Vol. 3